

A Climatological Analysis of the Linkages between Tropopause Polar Vortices, Cold Pools, and Cold Air Outbreaks over the Central and Eastern United States

KEVIN A. BIERNAT,^a LANCE F. BOSART,^a AND DANIEL KEYSER^a

^a *Department of Atmospheric and Environmental Sciences, University at Albany, State University of New York, Albany, New York*

(Manuscript received 12 June 2020, in final form 5 November 2020)

ABSTRACT: Coherent vortices in the vicinity of the tropopause, referred to as tropopause polar vortices (TPVs), may be associated with tropospheric-deep cold pools. TPVs and associated cold pools transported from high latitudes to middle latitudes may play important roles in the development of cold air outbreaks (CAOs). The purpose of this study is to examine climatological linkages between TPVs, cold pools, and CAOs occurring in the central and eastern United States. To conduct this study, 1979–2015 climatologies of TPVs and cold pools are constructed using the ERA-Interim dataset and an objective tracking algorithm, and are compared to a 1979–2015 climatology of CAOs occurring in six NCEI-defined climate regions over the central and eastern United States. The climatologies of TPVs and cold pools indicate that central and eastern North America is a preferred corridor for their equatorward transport, and that the occurrence frequency of TPVs and cold pools is higher over northern regions of the United States compared to southern regions of the United States. Correspondingly, there is a higher percentage of CAOs linked to cold pools associated with TPVs over northern regions of the United States (32.1%–35.7%) compared to southern regions of the United States (4.4%–12.5%). TPVs and cold pools contributing to CAOs form most frequently over northern Canada and the Canadian Archipelago, and generally move southeastward toward southern Canada and the northern United States. TPVs and cold pools contributing to CAOs tend to be statistically significantly colder and longer lived when compared to all TPVs and cold pools transported to middle latitudes.

KEYWORDS: North America; Cold air surges; Cold pools; Tropopause; Vortices

1. Introduction

TPVs are cold-core, coherent tropopause-based cyclonic vortices and material features characterized by a local minimum of dynamic tropopause (DT) potential temperature, a lowered DT, a cyclonic potential vorticity (PV) anomaly, radii of 100–1000 km, and lifetimes of days to months (e.g., Hakim 2000; Pyle et al. 2004; Hakim and Canavan 2005; Cavallo and Hakim 2009, 2010, 2012; Szapiro and Cavallo 2018). Pyle et al. (2004) referred to TPVs as coherent tropopause disturbances (CTDs), which dynamically represent the same features as TPVs, except that TPVs are typically required to spend a portion of their lifetimes in high latitudes (e.g., Cavallo and Hakim 2009, 2010), while CTDs are not. Longwave radiative cooling has been shown to be important for the maintenance and intensification of TPVs (e.g., Cavallo and Hakim 2009, 2010, 2012, 2013). Cavallo and Hakim (2010, 2012, 2013) show that there is a region of enhanced longwave radiative cooling on and just below the DT at the location of TPVs resulting from enhanced vertical gradients of water vapor between relatively moist tropospheric air beneath TPVs and relatively dry stratospheric air within TPVs. There is a decrease in longwave radiative cooling above the region of enhanced longwave radiative cooling. As a result, there is a positive vertical gradient in radiative heating within TPVs that can contribute to an increase in static stability and the concomitant production of cyclonic PV within TPVs that helps maintain and intensify TPVs (e.g., Cavallo and Hakim 2010, 2012, 2013).

TPVs have been shown to be dynamically important precursors to the development and intensification of extratropical cyclones (e.g., Hoskins et al. 1985, section 6; Uccellini et al. 1985;

Hakim et al. 1995; Bosart et al. 1996; Simmonds and Rudeva 2012) and jet streaks (e.g., Pyle et al. 2004). TPVs may also be dynamically important precursors to the development of CAOs, which are incursions of cold air masses into a region that result in an episode of anomalously low surface temperatures (e.g., Konrad 1996; Walsh et al. 2001; Cellitti et al. 2006). TPVs are cold-core features and are associated with anomalously cold air throughout the depth of the troposphere (e.g., Cavallo and Hakim 2010). Several studies show evidence of tropospheric-deep cold pools located within and beneath TPVs and upper-tropospheric cyclonic PV anomalies (e.g., Defant and Taba 1957; Boyle and Bosart 1983; Shapiro et al. 1987; Hakim et al. 1995; Papritz et al. 2019). Papritz et al. (2019) show that cooling air parcels trapped throughout the troposphere within and beneath TPVs can contribute to the formation of cold pools, and, along with Shapiro et al. (1987), show that exceptionally cold air that may be associated with these cold pools can contribute to the development of CAOs. Longwave radiative cooling from surface snow and ice cover (e.g., Curry 1983), and from ice crystals (e.g., Gotaas and Benson 1965; Curry 1983), liquid water droplets (e.g., Curry 1983), and low-level clouds (e.g., Curry 1983; Emanuel 2008) often found in the troposphere within cold air masses, may contribute to the cooling of cold pools (e.g., Turner and Gyakum 2011; Turner et al. 2013; Papritz et al. 2019). Although TPVs are not necessary for the development of CAOs, so long as the air mass associated with a CAO is cold enough, the exceptionally cold air that may be found beneath TPVs suggests that TPVs may be effective in triggering CAOs.

TPVs (e.g., Hakim and Canavan 2005; Cavallo and Hakim 2009, 2010, 2012; Szapiro and Cavallo 2018), and 500-hPa cyclones (e.g., Bell and Bosart 1989) and 500-hPa troughs (e.g., Sanders 1988; Lefevre and Nielsen-Gammon 1995), in which

Corresponding author: Kevin A. Biernat, kbiernat@albany.edu

DOI: 10.1175/MWR-D-20-0191.1

© 2021 American Meteorological Society. For information regarding reuse of this content and general copyright information, consult the [AMS Copyright Policy](#) (www.ametsoc.org/PUBSReuseLicenses).

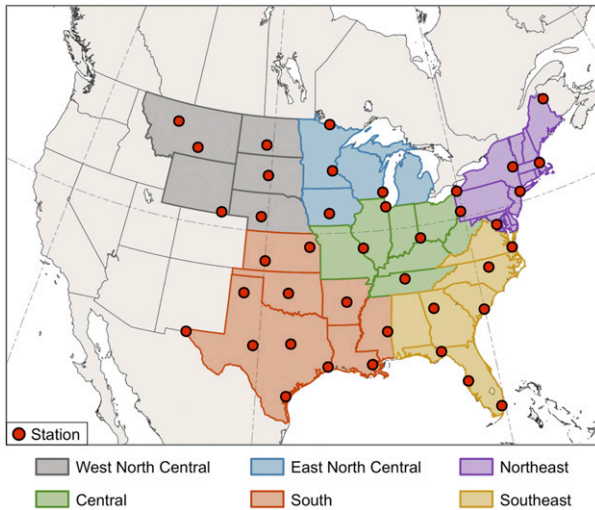


FIG. 1. NCEI climate regions (color shading) and GHCN-Daily stations (red dots) over the central and eastern United States used in Murphy (2017).

some TPVs may be embedded (e.g., Shapiro et al. 1987), have been shown to frequently occur over central and eastern North America. Similarly, CAOs have been shown to frequently occur over the same regions (e.g., Dallavalle and Bosart 1975; Konrad and Colucci 1989; Hartjenstein and Bleck 1991; Colle and Mass 1995; Konrad 1996; Walsh et al. 2001; Cellitti et al. 2006; Westby and Black 2015; Smith and Sheridan 2018). TPV track frequency is particularly high over northern Canada and the Canadian Archipelago (e.g., Cavallo and Hakim 2009, 2010, 2012; Szapiro and Cavallo 2018), where TPVs often meander slowly and intensify through longwave radiative cooling (e.g., Cavallo and Hakim 2009, 2010). Walsh et al. (2001) use a trajectory analysis to show that cold air parcels associated with CAOs over the central and eastern United States originate over high latitudes and often move slowly over northern Canada, where longwave radiative cooling may contribute to the cooling of these air parcels. The geographical coincidence of TPVs and cold air parcels associated with CAOs suggests that there may be a linkage between TPVs and the cold air parcels, such that TPVs may contribute to CAOs.

Research on the linkages between TPVs and CAOs has been a topic of recent interest. Papritz et al. (2019) examine linkages between CAOs occurring just south of the Fram Strait and TPVs, finding that 40% and 29% of the top 40 and 100 CAOs, respectively, are associated with TPVs. Lillo et al. (2020) show that a CAO occurring over the United States during late January and early February 2019 is linked to an intense TPV. The present study provides a complementary analysis of linkages between TPVs and CAOs by constructing 1979–2015 climatologies of TPVs and cold pools, which are compared to a 1979–2015 climatology of CAOs occurring in six NCEI-defined climate regions over the central and eastern United States, and examining the climatological linkages between TPVs, cold pools, and CAOs.

The remainder of this paper is organized as follows: section 2 presents the data and methodology used to construct the 1979–2015 climatologies of TPVs, cold pools, and CAOs, and to examine their mutual climatological linkages. Section 3

TABLE 1. GHCN-Daily stations used in Murphy (2017) for each NCEI climate region over the central and eastern United States. Number of stations in each climate region is given by N , which also represents the number of stations Murphy uses to identify CAOs for each climate region.

Regions	Stations (identifier in parentheses)
WNC ($N = 6$)	Billings, MT (KBIL) Bismarck, ND (KBIS) Cheyenne, WY (KCYS) Great Falls, MT (KGTF) North Platte, NE (KLBF) Pierre, SD (KPIR)
ENC ($N = 4$)	Des Moines, IA (KDSM) International Falls, MN (KINL) Milwaukee, WI (KMKE) Minneapolis, MN (KMSP)
Northeast ($N = 6$)	Albany, NY (KALB) Boston, MA (KBOS) Caribou, ME (KCAR) Erie, PA (KERI) New York, NY/LaGuardia (KLGA) Pittsburgh, PA (KPIT)
Central ($N = 4$)	Chicago, IL/Midway (KMDW) Cincinnati, OH (KCVG) Nashville, TN (KBNA) St. Louis, MO (KSTL)
South ($N = 12$)	Amarillo, TX (KAMA) Corpus Christi, TX (KCRP) Dodge City, KS (KDDC) El Paso, TX (KELP) Little Rock, AR (KLIT) Meridian, MS (KMEI) New Orleans, LA (KMSY) Oklahoma City, OK (KOKC) Port Arthur, TX (KBPT) San Angelo, TX (KSJT) Topeka, KS (KTOP) Waco, TX (KACT)
Southeast ($N = 8$)	Atlanta, GA (KATL) Charleston, SC (KCHS) Miami, FL (KMIA) Norfolk, VA (KORF) Raleigh, NC (KRDU) Tallahassee, FL (KTLH) Tampa, FL (KTPA) Washington, DC/Reagan National (KDCA)

discusses the climatologies, including the locations, seasonality, and characteristics of TPVs and cold pools, and examines the climatological linkages between TPVs, cold pools, and CAOs. Section 4 summarizes the results of the paper.

2. Data and methodology

a. Identification of TPVs and cold pools

All data used in this study for identifying TPVs and cold pools are from the ERA-Interim (Dee et al. 2011), downloaded at $0.5^\circ \times 0.5^\circ$ horizontal resolution. TPVs are tracked poleward of 30°N every 6 h during 1979–2015 utilizing an objective TPV tracking algorithm developed by Szapiro and Cavallo (2018)

TABLE 2. Number of unique stations that can be used to identify CAOs for each climate region, and number and normalized number of CAOs for each climate region during 1979–2015. The normalized number of CAOs is rounded to the nearest whole number.

	WNC	ENC	Northeast	Central	South	Southeast
Number of unique stations that can identify CAOs	13	14	12	16	20	17
Number of CAOs	145	126	137	152	227	179
Normalized number of CAOs	167	135	171	143	170	158

called TPVTrack. TPVTrack uses potential temperature, zonal and meridional winds, and the vertical component of relative vorticity on the DT (2-PVU surface) as input variables. At each time step, the DT potential temperature field is segmented into regions. Each region, representing a candidate TPV, is defined such that there is a DT potential temperature minimum and all locations in the region possess positive values of the vertical component of DT relative vorticity. The regions are advected in space and time with use of the DT zonal and meridional winds. The extent of overlap between advected regions is used to determine which regions are connected in space and time to create TPV tracks. TPVTrack calculates the area of each region at each time step along the TPV tracks and outputs the radius of a circle with an equivalent area. The radius information will be used later in the present study. The location or center of a TPV is the location of the DT potential temperature minimum of the TPV. For detailed information on TPVTrack, the reader is referred to Szapiro and Cavallo (2018).

To track cold pools, TPVTrack is modified by only changing the input variables to 1000–500-hPa thickness, 700-hPa zonal and meridional winds, and 1000–500-hPa thermal vorticity, which is calculated by subtracting the vertical component of

1000-hPa relative vorticity from the vertical component of 500-hPa relative vorticity. The 1000–500-hPa thickness field is used because it can represent the structure of the thermal field throughout the troposphere within and beneath TPVs, which often extend downward to 500 hPa or lower (e.g., Cavallo and Hakim 2010). The 1000–500-hPa thermal vorticity field is used because positive values of 1000–500-hPa thermal vorticity can represent regions of relatively cold air associated with cold pools. The 700-hPa zonal and meridional winds are used because these winds are located approximately at the midpoint of the 1000–500-hPa layer. Like TPVs, cold pools are tracked poleward of 30°N every 6 h during 1979–2015. With the modified TPVTrack for cold pool tracking, the 1000–500-hPa

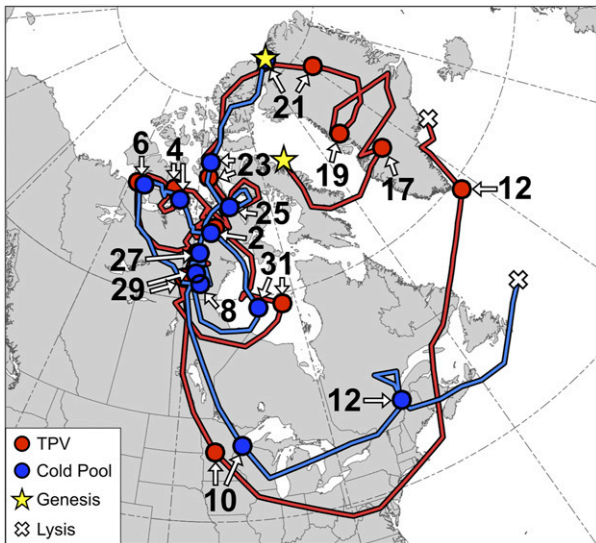


FIG. 2. Tracks of TPV (red) every 6 h from 0600 UTC 15 Dec 1981 to 0000 UTC 13 Jan 1982 and cold pool (blue) every 6 h from 1800 UTC 20 Dec 1981 to 1800 UTC 13 Jan 1982. Stars denote locations of genesis, crosses denote locations of lysis, and red and blue dots denote 0000 UTC positions of TPV and cold pool, respectively, every 48 h. Numbers adjacent to arrows pointing toward dots denote dates of the 0000 UTC positions of the TPV and cold pool.

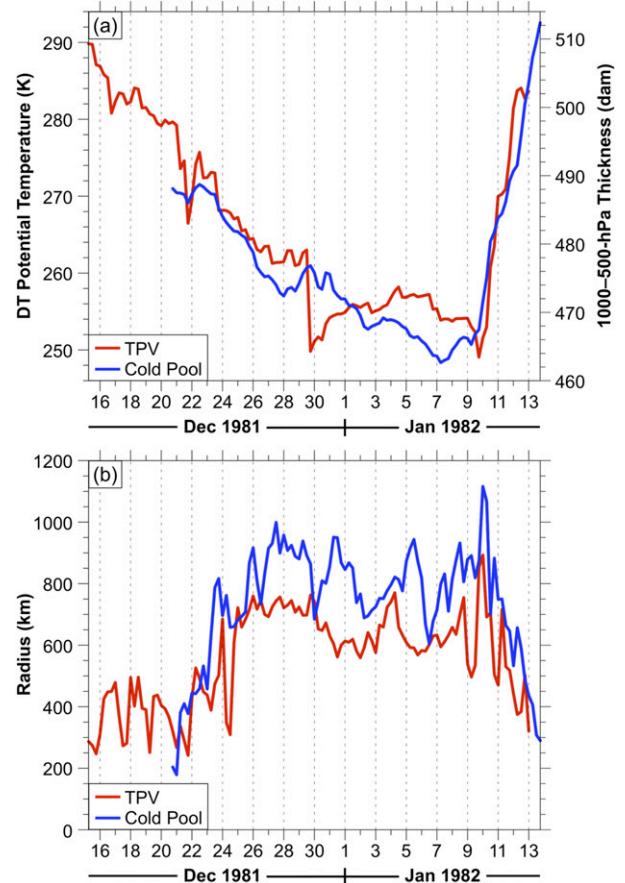


FIG. 3. (a) Time series of minimum DT potential temperature of TPV (K, red) and minimum 1000–500-hPa thickness of cold pool (dam, blue) and (b) time series of TPV radius (km, red) and cold pool radius (km, blue), every 6 h for same respective time periods as in Fig. 2.

TABLE 3. Mean values of the mean radius (km) and maximum radius (km) during the lifetime of all TPVs and cold pools during 1979–2015, and of TPVs and cold pools transported to middle latitudes during 1979–2015.

	All		Transported to middle latitudes	
	TPVs	Cold pools	TPVs	Cold pools
Mean radius (km)	297.2	388.6	321.3	434.6
Max radius (km)	442.8	548.4	490.3	619.6

thickness field is segmented into regions. Each region, representing a candidate cold pool, is defined such that there is a 1000–500-hPa thickness minimum and all locations in the region possess positive values of 1000–500-hPa thermal vorticity. The 700-hPa zonal and meridional winds are used to advect the regions. As described for TPVs, the modified TPVTrack outputs radius information for the cold pools, which will be used later in the present study. The location or center of a cold pool is the location of the 1000–500-hPa thickness minimum of the cold pool. To test the modified TPVTrack for cold pool tracking, several manual cold pool tracks, which are constructed by manually following the location of the 1000–500-hPa thickness minimum of the cold pools, are compared to their corresponding objective cold pool tracks. The manual and objective cold pool tracks are found to be very similar (not shown).

TPVs and cold pools are filtered by requiring them to last at least 2 days and spend at least 6 h poleward of 60°N. Cavallo and Hakim (2009) require that TPVs last at least 2 days and spend at least 60% of their lifetimes poleward of 65°N. A more relaxed latitude criterion is imposed in the present study

because the primary interest is on TPVs transported from high latitudes (>60°N) to middle latitudes (30°–60°N), where they may be associated with CAOs. Thus, TPVs and cold pools that may not spend a large portion of their lifetimes in high latitudes, but may still be associated with CAOs, can be identified.

b. Identification of CAOs

The present study adapts the CAO identification methodology of Murphy (2017) to construct a climatology of CAOs occurring over the central and eastern United States during 1979–2015. Daily minimum temperature data are extracted from stations within the Global Historical Climatology Network (GHCN)-Daily dataset (Menne et al. 2012) that are relatively evenly distributed across six climate regions defined by NCEI over the central and eastern United States, which include West North Central (WNC), East North Central (ENC), Northeast, Central, South, and Southeast (Fig. 1 and Table 1). The stations are the same as those used by Murphy, who chose these stations because of their superior temporal coverage during 1948–2015, which is the period he used to identify CAOs. A CAO is defined to occur in the present study when a given station and at least one other station located within 700 km of the given station experience 3 or more consecutive days where daily minimum temperatures are less than or equal to the 31-day centered moving average of the 5th-percentile minimum temperature for those days (based on a 1979–2015 climatology) and share at least one overlapping day. Each CAO is counted toward the regions in which the stations involved in the CAO identification are located. If two separate CAOs identified for a region share at least one overlapping day, the CAOs are grouped together to create a single CAO for that region. The

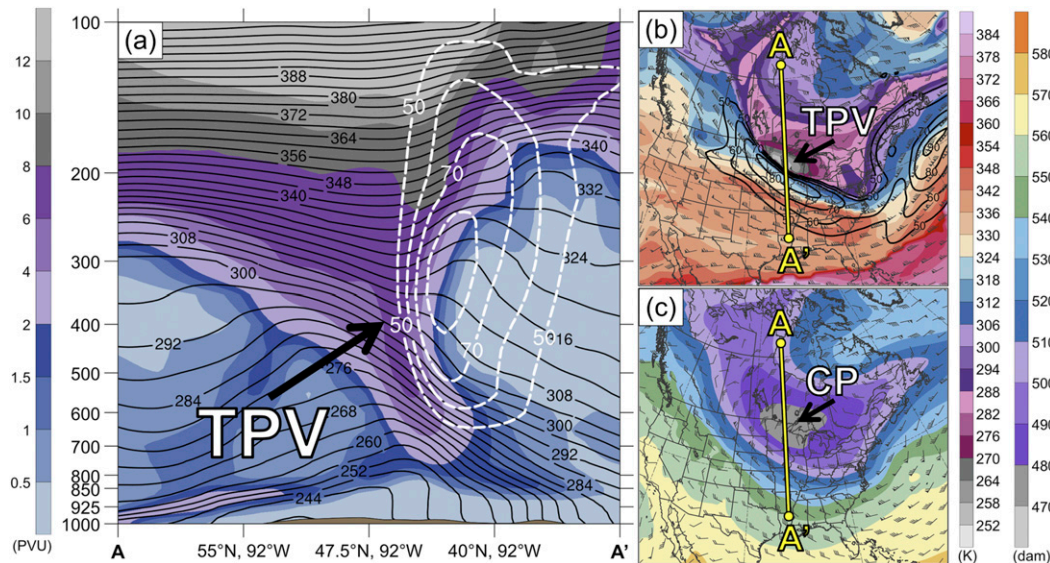


FIG. 4. (a) Cross section along line AA' of PV (PVU, shading), potential temperature (K, black), and wind speed (dashed white contours every 10 m s⁻¹, beginning at 50 m s⁻¹); (b) DT (2-PVU surface) potential temperature (K, shading), wind speed (black contours every 10 m s⁻¹, beginning at 50 m s⁻¹), and wind (m s⁻¹, flags and barbs); and (c) 1000–500-hPa thickness (dam, shading) and 700-hPa wind (m s⁻¹, flags and barbs). Yellow line in (b) and (c) denotes location of cross section AA'. Labels “TPV” and “CP” denote locations of TPV and cold pool, respectively. Analyses are for 0000 UTC 10 Jan 1982. Data source: ERA-Interim.

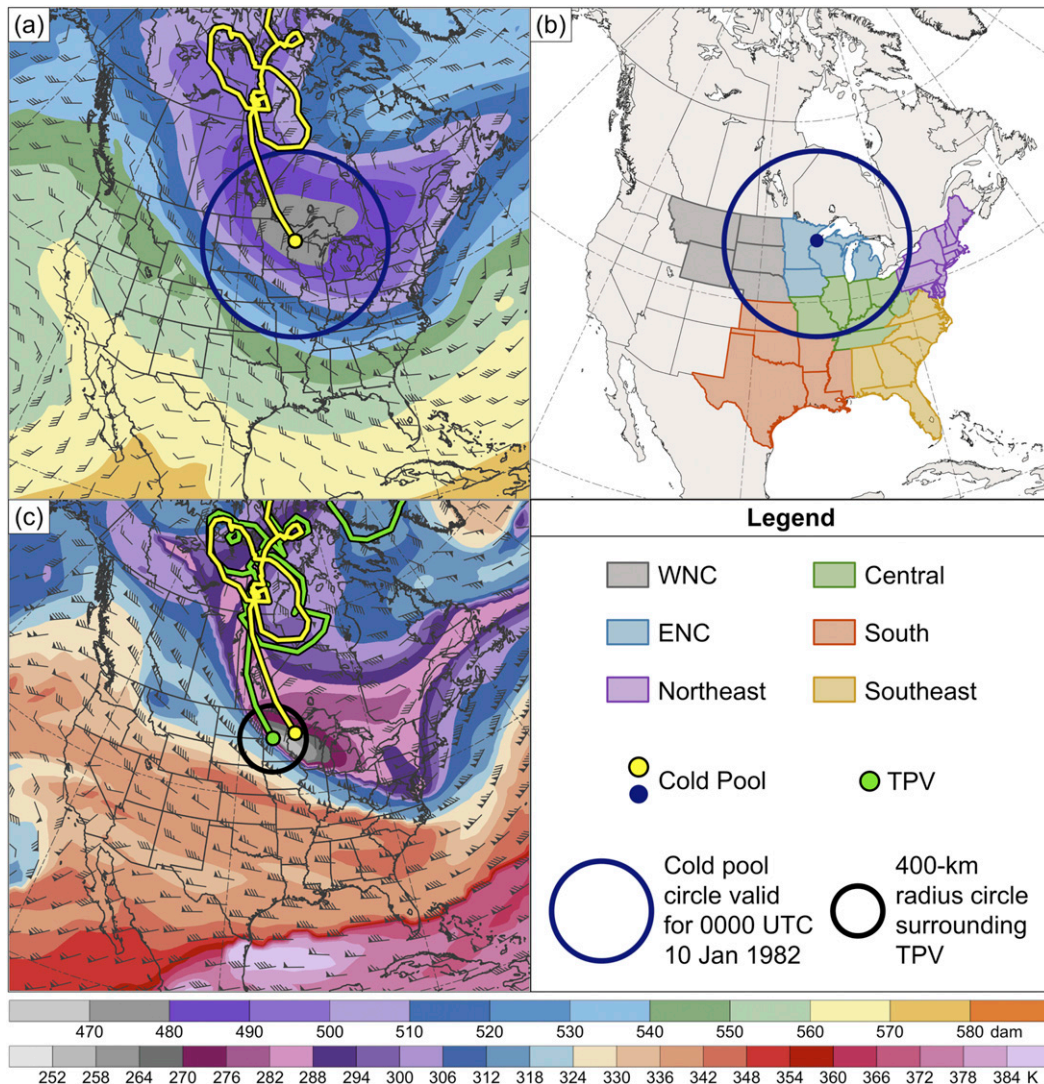


FIG. 5. (a) 1000–500-hPa thickness (dam, shading), 700-hPa wind ($m s^{-1}$, flags and bars), cold pool track (yellow line), and cold pool circle (blue circle) surrounding cold pool center (yellow dot) at 0000 UTC 10 Jan 1982. The cold pool circle has a radius of 1116 km at 0000 UTC 10 Jan 1982. (b) NCEI climate regions (color shading) and same cold pool circle as in (a) surrounding cold pool center (blue dot) at 0000 UTC 10 Jan 1982. (c) DT (2-PVU surface) potential temperature (K, shading) and wind ($m s^{-1}$, flags and bars), TPV and cold pool tracks (green and yellow lines, respectively), position of TPV center and cold pool center (green and yellow dots, respectively), and 400-km radius circle (black circle) surrounding TPV center at 0000 UTC 10 Jan 1982. TPV and cold pool tracks are repeated from Fig. 2 from the respective times of genesis of the TPV and cold pool to 0000 UTC 10 Jan 1982. Data source: ERA-Interim.

CAO definition in the present study is the same as in Murphy (2017) except that Murphy only uses stations located within a given region to identify CAOs for the given region, while in the present study, all unique stations that are located within 700 km of the stations in a given region can be used to identify CAOs for the given region. Thus, more stations can be used to identify CAOs for a given region in the present study (Table 2) compared to in Murphy (2017) (Table 1).

The 700-km threshold is chosen because it is large enough such that there are at least two stations (the average is ~6 stations) located within 700 km of each station except Great Falls,

MT. Only one station (Billings, MT) is located within 700 km of Great Falls, MT. The 700-km threshold is also comparable to a spatial criterion used by Smith and Sheridan (2018) for CAO identification that requires that at least three contiguous stations, which are spaced roughly 500–700 km apart, simultaneously meet CAO criteria imposed in their study.

c. Identification of linkages between TPVs, cold pools, and CAOs

All CAOs during 1979–2015, and all TPVs and cold pools transported to middle latitudes, i.e., TPVs and cold pools that

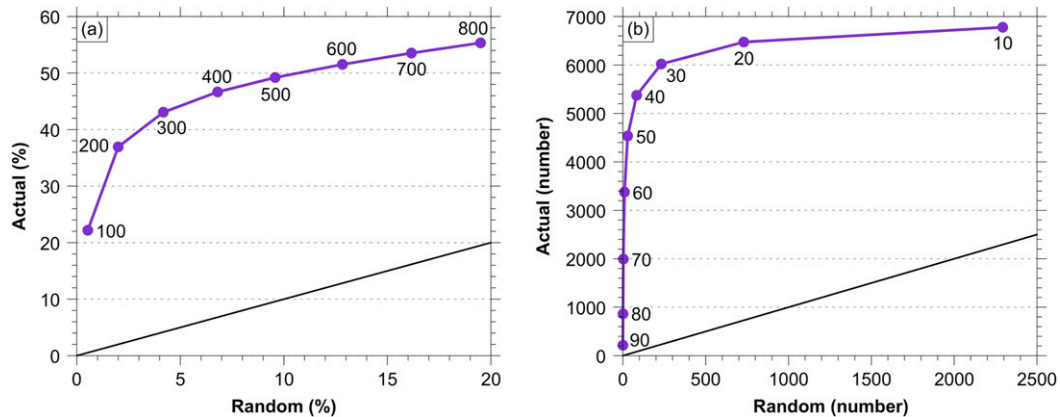


FIG. 6. (a) Mean TPV–cold pool match percentage for the random climatology vs mean TPV–cold pool match percentage for the actual climatology, for distance thresholds of 100 to 800 km, every 100 km (purple line and dots). For reference, the black line indicates where the mean TPV–cold pool match percentage for the random climatology equals the mean TPV–cold pool match percentage for the actual climatology. (b) Number of TPV–cold pool matches for the random climatology vs number of TPV–cold pool matches for the actual climatology, for TPV–cold pool match percentage thresholds of 90% to 10%, every 10% (purple line and dots), when using a distance threshold of 400 km. For reference, the black line indicates where the number of TPV–cold pool matches for the random climatology equals the number of TPV–cold pool matches for the actual climatology.

move equatorward of 60°N after being located poleward of 60°N, during 1979–2015 are considered when identifying linkages between TPVs, cold pools, and CAOs. A CAO that occurs over all six climate regions during 9–12 January 1982 is used to illustrate how these linkages are identified. This CAO is linked to a TPV and cold pool that spend much of their lifetimes meandering in tandem with each other over Canada during late December 1981 and early January 1982, before moving equatorward into and then eastward across the northern United States (Fig. 2). The TPV and cold pool concomitantly intensify over Canada during late December 1981 and early January 1982, with the TPV obtaining a minimum DT potential temperature of ~ 249 K on 9 January 1982 and the cold pool obtaining a minimum 1000–500-hPa thickness of ~ 463 dam on 7 January 1982 (Fig. 3a). The TPV and cold pool grow in size during late December 1981 as they intensify, and then oscillate in size (Fig. 3b). The TPV and cold pool have a mean radius of 557 and 740 km, respectively, and a maximum radius of 893 and 1116 km, respectively, during their respective lifetimes, indicating that the TPV and cold pool are subsynoptic in scale and that the cold pool is larger than the TPV, as is typical in the 1979–2015 climatologies of TPVs and cold pools (Table 3). A meridional cross section through the TPV and cold pool at 0000 UTC 10 January 1982 (Figs. 4a–c) shows that the TPV extends downward to ~ 750 hPa and is associated with a tropopause fold (e.g., Reed and Danielsen 1959; Danielsen 1968; Keyser and Shapiro 1986, sections 2a,b) and an intense jet streak (Figs. 4a,b). There is a notable upward bowing of isentropes throughout the troposphere within and beneath the TPV (Fig. 4a), illustrative of the cold pool (Fig. 4c) associated with the TPV, with low surface potential temperature values extending away from the core of the TPV (Fig. 4a). The large spatial overlap and temporal coincidence of the TPV and cold pool (Fig. 2), and the concomitant intensification of the TPV

and cold pool (Fig. 3a), suggest that the TPV and cold pool are dynamically linked.

The January 1982 CAO is clearly linked to a cold pool associated with TPVs. To identify all CAOs linked to cold pools associated with TPVs, CAOs linked to cold pools are first identified. CAOs linked to cold pools are identified by requiring that a cold pool circle with a radius given by TPVTrack surrounding the cold pool center intersect with at least one grid point on a $0.5^\circ \times 0.5^\circ$ grid within a climate region experiencing a CAO for at least one 6-h time step during the CAO (Figs. 5a,b). The cold pool circle at 0000 UTC 10 January 1982 contains all six regions except Southeast (Figs. 5a,b), but the cold pool circle at later times during the CAO does contain Southeast (not shown). Thus, the January 1982 CAO qualifies as a CAO linked to a cold pool for all six regions. Not all CAOs linked to cold pools are caused entirely by the cold pools. Some cold pools may only contribute to a portion of a CAO since some cold pools may move progressively across a region. In addition, some cold pools may only contribute to a CAO over a portion of a region, especially since cold pools tend to be subsynoptic in scale (Table 3). Some cold pools may be embedded in broader areas of cold air (e.g., larger-scale 1000–500-hPa thickness troughs) that also contribute to the CAOs.

Once CAOs linked to cold pools are identified, cold pools associated with TPVs and TPVs associated with cold pools are identified. A cold pool and a TPV should be located within a sufficient distance threshold of each other for a sufficient percentage of their respective lifetimes in order for them to be associated with each other. To determine a sufficient distance threshold, an approach used by Papritz et al. (2014) to find an optimal percentage of overlap between precipitation objects and fronts in order to attribute precipitation to fronts is adapted. TPV–cold pool matches are determined for distance thresholds of 100 to 800 km, every 100 km, for both the actual

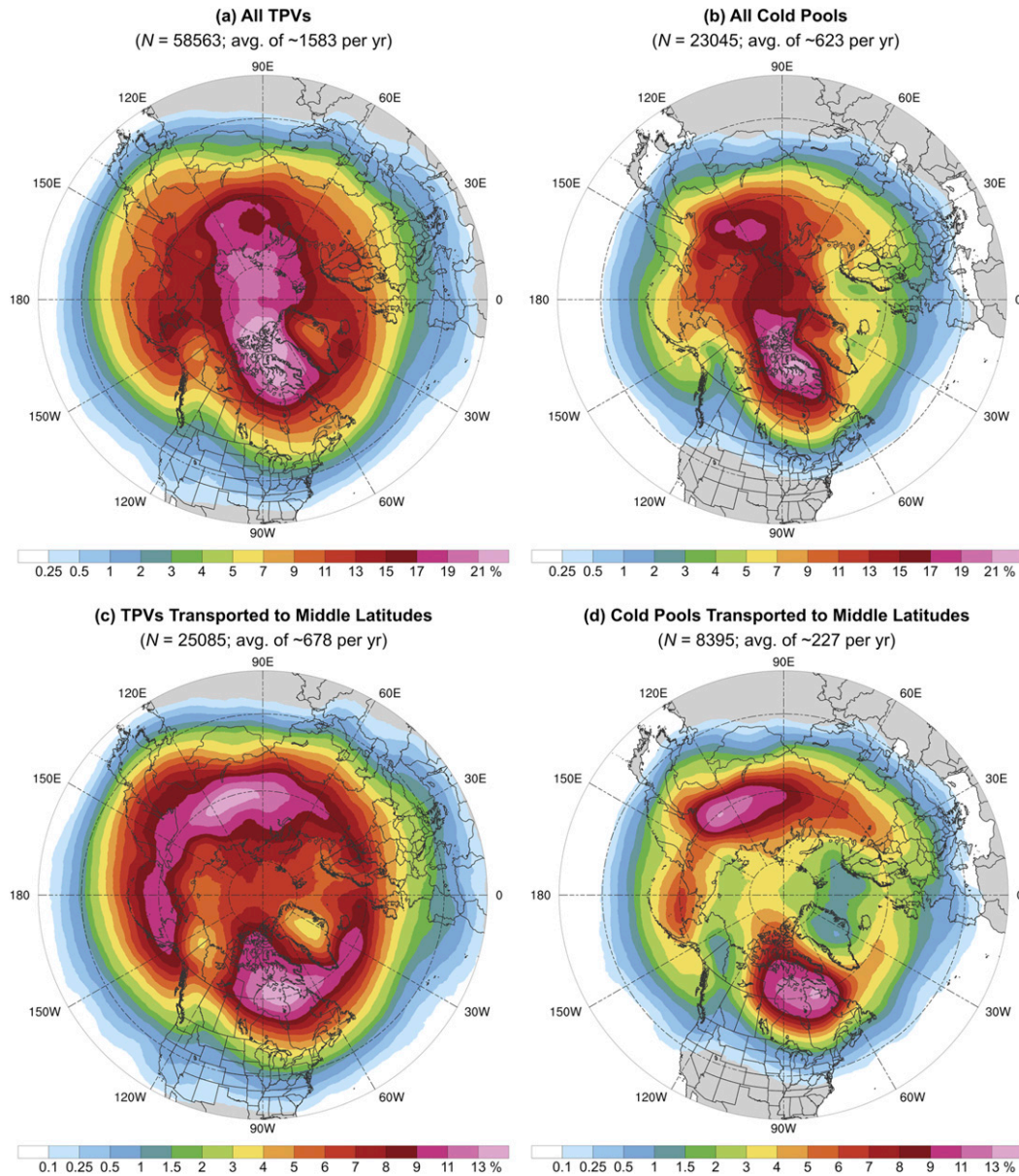


FIG. 7. Occurrence frequency (%) of (a) all TPVs, (b) all cold pools, (c) TPVs transported to middle latitudes (equatorward of 60°N), and (d) cold pools transported to middle latitudes (equatorward of 60°N), calculated following Szapiro and Cavallo (2018) by determining the percentage of time steps during 1979–2015 a given grid point (using a 0.5° grid) is located within the radius of these respective features.

climatology of cold pools and for a random climatology. In this random climatology, a time period during 1979–2015 is randomly chosen for each cold pool that 1) begins in the same month in which the cold pool forms and 2) contains the same number of time steps as the lifetime of the cold pool. For each cold pool, TPVs that exist in the same time period as the cold pool for the actual climatology and in the randomly chosen time period for the random climatology are determined. For each TPV–cold pool combination, the percentage of the lifetime of the cold pool and the percentage of the lifetime of the TPV for which the cold pool

center and TPV center are located within the distance threshold is determined, and the average of the two percentages (hereafter referred to as the “TPV–cold pool match percentage”) is calculated. The TPV–cold pool combination for which the TPV–cold pool match percentage is highest and greater than zero is chosen as the TPV–cold pool match, and the TPV–cold pool match percentage is retained. If there is no TPV–cold pool match, a TPV–cold pool match percentage of zero is retained. The mean of all retained TPV–cold pool match percentage values (total number of values is 8395, which is the total number of cold pools) is calculated for each distance

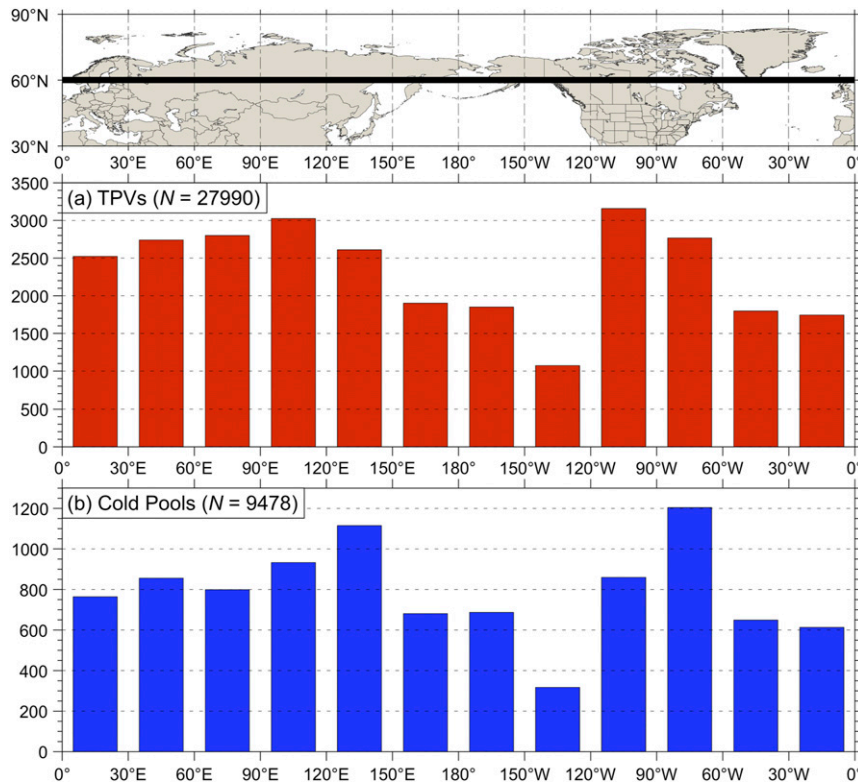


FIG. 8. Histograms showing the total number of instances in which (a) TPVs and (b) cold pools cross equatorward of 60°N (black line on map) for each 30° longitudinal bin globally during 1979–2015. An individual TPV and an individual cold pool may be counted more than once if they cross equatorward of 60°N after returning poleward of 60°N.

threshold for the actual climatology and for the random climatology.

By increasing the distance threshold, both the mean TPV–cold pool match percentage for the actual climatology and for the random climatology will increase (Fig. 6a). The optimal choice of threshold would be the threshold beyond which the mean TPV–cold pool match percentage for the actual climatology and for the random climatology increase by the same amount, i.e., any additional increase in the mean TPV–cold pool match percentage would be indistinguishable to an increase in the mean TPV–cold pool match percentage resulting from random chance. Figure 6a shows that when the distance threshold is increased beyond 400 km, the mean TPV–cold pool match percentage for the actual climatology increases by either almost the same amount or by a lower amount compared to the mean TPV–cold pool match percentage for the random climatology, indicating that 400 km is an appropriate distance threshold.

Now that the distance threshold of 400 km is chosen, an optimal TPV–cold pool match percentage threshold that should be exceeded when using the 400-km distance threshold is determined, which indicates how often a cold pool center and a TPV center should be located within 400 km of each other in order for the cold pool and TPV to be considered associated with each other. To find the optimal TPV–cold pool match percentage threshold, the number of TPV–cold pool

matches for which the TPV–cold pool match percentage exceeds thresholds ranging from 90% to 10%, every 10%, for the actual climatology and for the random climatology is determined. By decreasing the TPV–cold pool match percentage threshold, both the number of TPV–cold pool matches for the actual climatology and for the random climatology will increase (Fig. 6b). The optimal choice of threshold would be that threshold beyond which the number of TPV–cold pool matches for the actual climatology and for the random climatology increase by the same amount, i.e., any additional increase in the number of TPV–cold pool matches would be indistinguishable to an increase in the number of TPV–cold pool matches resulting from random chance. Figure 6b shows that when the TPV–cold pool match percentage threshold is decreased below 30%, the number of TPV–cold pool matches for the actual climatology increases by either almost the same amount or by a lower amount compared to the number of TPV–cold pool matches for the random climatology, indicating that 30% is an appropriate TPV–cold pool match percentage threshold. Cold pools associated with TPVs and TPVs associated with cold pools are therefore those TPV–cold pool matches for which the TPV–cold pool match percentage exceeds 30% when using a distance threshold of 400 km.

The TPV and cold pool involved in the January 1982 CAO are within 400 km of each other at 0000 UTC 10 January 1982 and throughout much of their lifetimes (Fig. 5c), having a

TABLE 4. Number, normalized number, and percentage of CAOs linked to cold pools for each climate region. Percentage of CAOs linked to cold pools is defined as the number of CAOs linked to cold pools divided by the number of CAOs (given in Table 2). The normalized number of CAOs linked to cold pools is rounded to the nearest whole number.

	WNC	ENC	Northeast	Central	South	Southeast
Number	62	55	56	25	12	20
Normalized number	72	59	70	23	9	18
Percentage	42.8	43.7	40.9	16.4	5.3	11.2

TPV–cold pool match percentage of 75.7%. Thus, the TPV and cold pool are associated with each other. Once cold pools associated with TPVs are identified, CAOs linked to cold pools associated with TPVs can be identified. Since the cold pool involved in the January 1982 CAO is a cold pool associated with a TPV, this CAO qualifies as a CAO linked to a cold pool associated with a TPV for the same climate regions in which this CAO qualifies as a CAO linked to a cold pool, which are all six regions.

3. Results

a. Locations of TPVs and cold pools

Areas of high occurrence frequency of all TPVs (Fig. 7a) and all cold pools (Fig. 7b) during 1979–2015 are found over northern Canada, the Canadian Archipelago, Eurasia, and the Arctic, which are also regions of high TPV occurrence shown in Hakim and Canavan (2005), Cavallo and Hakim (2009, 2010, 2012), and Szapiro and Cavallo (2018). Cold pool occurrence frequency is relatively low when compared to TPV occurrence frequency over the open waters of the Norwegian Sea (Figs. 7a,b), from which surface sensible heat fluxes may weaken or destroy cold pools (e.g., Papritz et al. 2019) but may have little to no influence on TPVs. The lower total number of cold pools (23045) compared to TPVs (58563) likely is a consequence of the 1000–500-hPa thickness field, from which cold pools are identified, being smoother than the DT potential temperature field, from which TPVs are identified, resulting in fewer trackable minima of 1000–500-hPa thickness than minima of DT potential temperature.

Maxima of occurrence frequency of TPVs and cold pools transported to middle latitudes are found over central and eastern North America and over central and eastern Eurasia (Figs. 7c,d). There are also maxima in the number of instances in which TPVs and cold pools cross into middle latitudes over central and eastern North America and over central and eastern Eurasia, and there is a minimum in the number of instances in which TPVs and cold pools cross into middle

latitudes over the eastern North Pacific and western North America (Figs. 8a,b). Climatologically favored upper-tropospheric ridging over the eastern North Pacific and western North America, which may prevent the equatorward transport of TPVs and cold pools in these regions, may aid in the equatorward transport of TPVs and cold pools downstream over central and eastern North America (e.g., Shapiro et al. 1987; Colle and Mass 1995; Hakim et al. 1995; Konrad 1996), where they may play important roles in the development of CAOs.

b. Linkages between TPVs, cold pools, and CAOs

Linkages between TPVs, cold pools, and CAOs are now examined. Only TPVs and cold pools transported to middle latitudes are considered. Starting with the 1979–2015 climatology of CAOs, regional variability in the number of CAOs is found across the six climate regions (Table 2). Differences in the number of unique stations that can be used to identify CAOs for each region (Table 2) likely contribute to the regional variability, as regions with fewer unique stations tend to have fewer CAOs than regions with more unique stations (Table 2). To illustrate the impact of the number of unique stations on the number of CAOs for each region, the number of CAOs for each region is normalized by multiplying the number of CAOs by 15 (the median number of unique stations for all of the regions) and then dividing by the number of unique stations for the region. The normalized number of CAOs is found to vary less across the regions (135–171) compared to the raw number of CAOs (126–227) (Table 2). In the upcoming results, the number of CAOs linked to cold pools and the number of CAOs linked to cold pools associated with TPVs are normalized following the same normalization procedure just described.

In terms of CAOs linked to cold pools, there is a higher number and normalized number of CAOs linked to cold pools over northern regions of the United States (i.e., WNC, ENC, and Northeast) compared to southern regions of the United States (i.e., Central, South, and Southeast) (Table 4). There is a moderate percentage of CAOs linked to cold pools over northern regions of the United States (40.9%–43.7%) and a

TABLE 5. Number, normalized number, and percentage of CAOs linked to cold pools associated with TPVs for each climate region. Percentage of CAOs linked to cold pools associated with TPVs is defined as the number of CAOs linked to cold pools associated with TPVs divided by the number of CAOs (given in Table 2). The normalized number of CAOs linked to cold pools associated with TPVs is rounded to the nearest whole number.

	WNC	ENC	Northeast	Central	South	Southeast
Number	51	45	44	19	10	15
Normalized number	59	48	55	18	8	13
Percentage	35.2	35.7	32.1	12.5	4.4	8.4

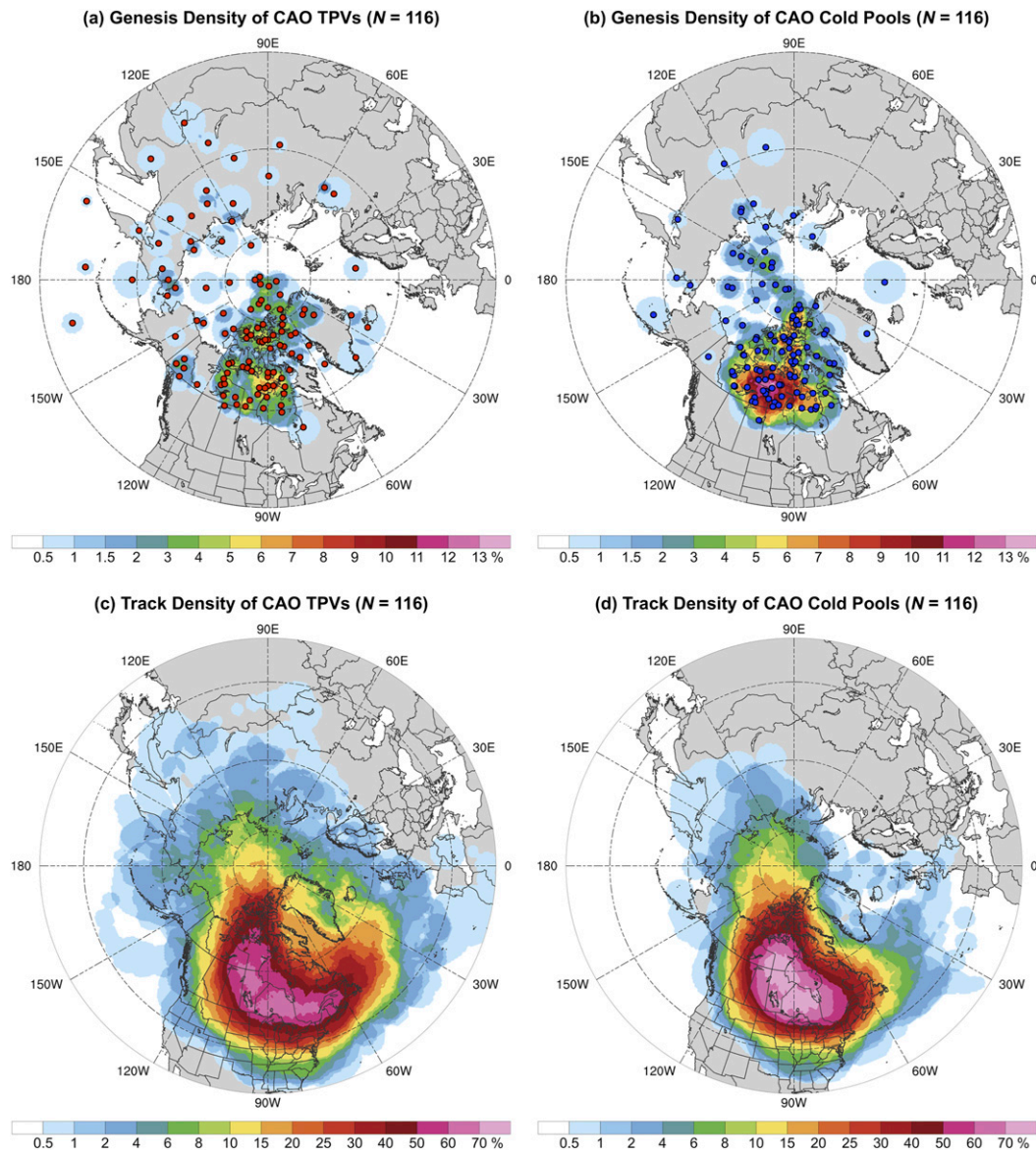


FIG. 9. Genesis density of (a) CAO TPVs and (b) CAO cold pools for all climate regions, shaded according to the percentage of these respective features for which a given grid point (using a 0.5° grid) is located within the radius of these respective features at the time of genesis of these respective features. Locations of (a) CAO TPVs (red dots) and (b) CAO cold pools (blue dots) at the time of genesis of these respective features are also shown. Track density of aforementioned (c) CAO TPVs and (d) CAO cold pools, shaded according to the percentage of these respective features for which a given grid point (using a 0.5° grid) is located within the radius of these respective features at any time during the lifetime of these respective features. If an individual CAO TPV or individual CAO cold pool impacts multiple regions, that CAO TPV or CAO cold pool is only counted once in the total count of CAO TPVs [given by the value of N in (a) and (c)] and CAO cold pools [given by the value of N in (b) and (d)], respectively.

lower percentage over southern regions of the United States (5.3%–16.4%) (Table 4).

In terms of cold pools associated with TPVs and TPVs associated with cold pools, 6020 cold pools out of the total 8395 cold pools, or 71.7%, are associated with TPVs, and 6020 TPVs out of the total 25 085 TPVs, or 24.0%, are associated with cold pools. The higher total number of TPVs compared to cold

pools contributes to the percentage of TPVs associated with cold pools being lower. Some TPVs being too small or too weak to be associated with a cold pool and some TPVs being associated with a thickness trough that is not trackable as a cold pool may also contribute to the percentage of TPVs associated with cold pools being lower. The cold pools and TPVs that are associated with each other are located within 400 km of each

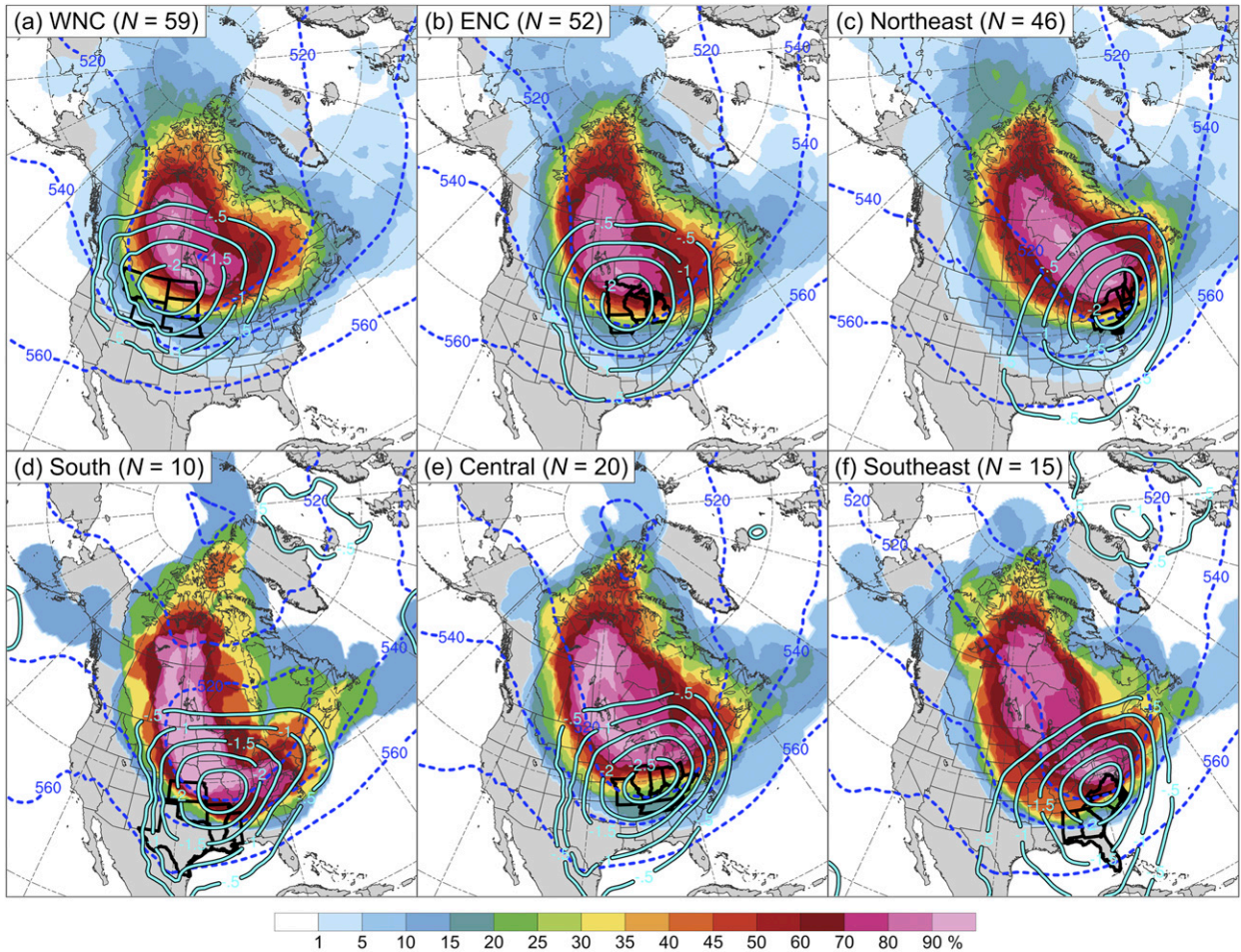


FIG. 10. Track density of CAO cold pools for the (a) WNC, (b) ENC, (c) Northeast, (d) South, (e) Central, and (f) Southeast regions, shaded according to the percentage of CAO cold pools for which a given grid point (using a 0.5° grid) is located within the radius of the CAO cold pools at any time during the lifetime of the CAO cold pools. Composite 1000–500-hPa thickness (every 20 dam, dashed blue contours) and composite negative values of standardized anomaly of 1000–500-hPa thickness (every 0.5σ , solid cyan contours) at t_{lowest} (defined in text in section 3c). States in each climate region are outlined in thick black. The same CAO cold pool can impact multiple regions, and thus the same CAO cold pool can be included in the total count of CAO cold pools (given by the value of N in each panel) for multiple regions.

other for a higher average percentage of the lifetime of the cold pools compared to the TPVs (72.7% vs 51.7%), which likely relates to the cold pools having a shorter average lifetime compared to the TPVs (6.9 vs 10.2 days).

Finally, in terms of CAOs linked to cold pools associated with TPVs, there is a higher number, normalized number, and percentage of CAOs linked to cold pools associated with TPVs over northern regions of the United States compared to southern regions of the United States (e.g., 32.1%–35.7% vs 4.4%–12.5%) (Table 5). The higher number, normalized number, and percentage of CAOs linked to cold pools (Table 4) and CAOs linked to cold pools associated with TPVs (Table 5) over northern regions of the United States compared to southern regions of the United States is a consequence of the higher occurrence frequency of TPVs and cold pools over northern regions of the United

States compared to southern regions of the United States (Figs. 7c,d).

c. Locations of TPVs and cold pools involved in CAOs

For CAOs linked to cold pools associated with TPVs, the locations of the TPVs (hereafter CAO TPVs) and cold pools (hereafter CAO cold pools) are examined for all climate regions in terms of genesis density and track density. CAO TPVs most frequently form over northern Canada, the Canadian Archipelago, and the adjacent Arctic, but also form over Siberia and the North Pacific (Fig. 9a). The Canadian Archipelago was also shown by Cavallo and Hakim (2009) to be a region of particularly high occurrence of TPV genesis. CAO cold pools also most frequently form over northern Canada, the Canadian Archipelago, and the adjacent Arctic (Fig. 9b), but less often form over Siberia and

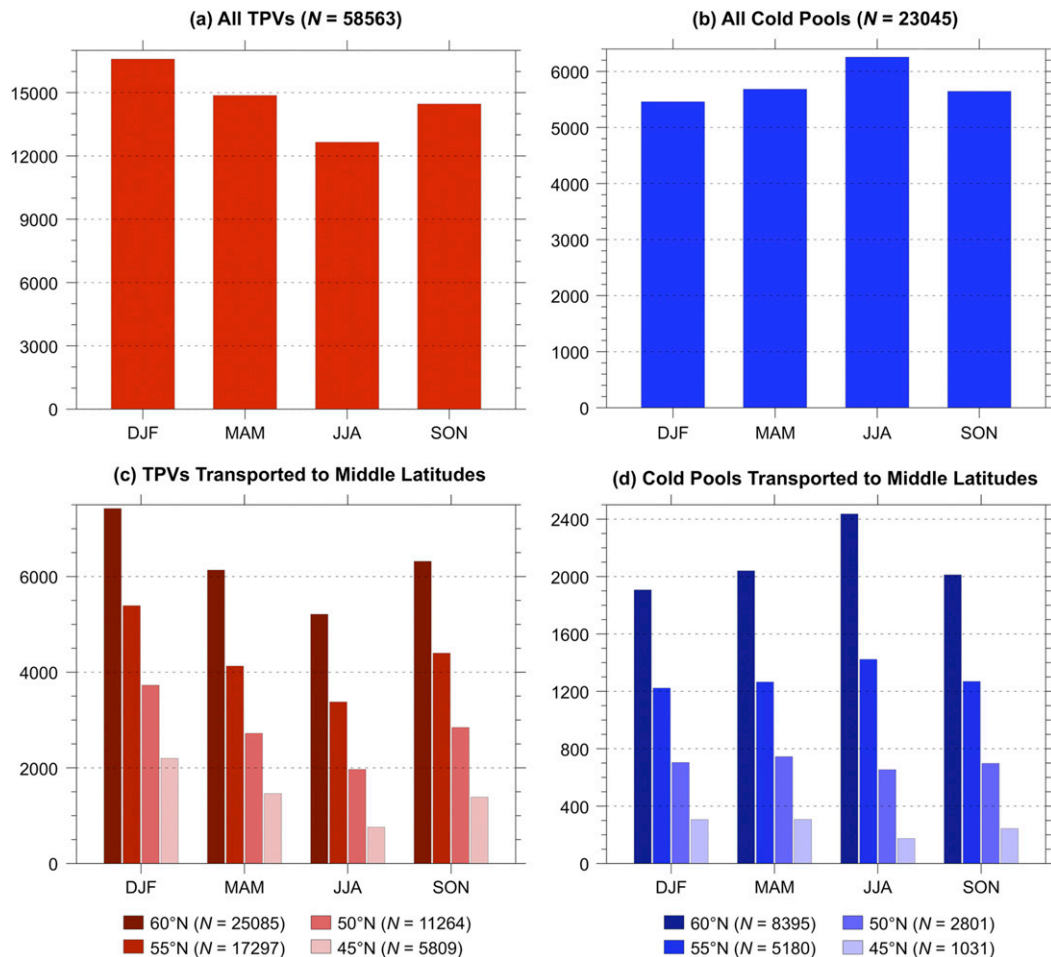


FIG. 11. Number of (a) all TPVs and (b) all cold pools for each season during 1979–2015. Number of (c) TPVs and (d) cold pools transported equatorward of crossing latitudes ranging from 60° to 45°N, every 5°, for each season during 1979–2015, where each bar is colored according to the crossing latitude. The conventional definition of meteorological seasons is adopted, where winter denotes December–February (DJF), spring denotes March–May (MAM), summer denotes June–August (JJA), and autumn denotes September–November (SON). TPVs and cold pools are separated into each season based on the month of their genesis date.

the North Pacific compared to CAO TPVs (cf. Figs. 9a,b). CAO TPVs and CAO cold pools do not always form simultaneously (e.g., Fig. 2), as some TPVs may not become associated with a cold pool until they attain sufficient strength. CAO TPVs and CAO cold pools follow a similar preferred pathway once over Canada, generally moving southeastward toward southern Canada and the northern United States, and then eastward toward the North Atlantic (Figs. 9c,d). Upper-tropospheric ridges and ridge amplification over the eastern North Pacific and western North America likely contribute to the equatorward transport of CAO TPVs and CAO cold pools across Canada (e.g., Shapiro et al. 1987; Colle and Mass 1995; Hakim et al. 1995).

Preferred areas impacted by CAO cold pools are now examined for each climate region in terms of track density. For each CAO cold pool and region, the time period during which the cold pool circle surrounding the cold pool center intersects the region during the CAO is determined, and the time during

this period at which the 1000–500-hPa thickness averaged across the region is lowest (hereafter t_{lowest}) is identified. The 1000–500-hPa thickness and the standardized anomaly of 1000–500-hPa thickness at t_{lowest} are composited for the CAO cold pools impacting each region. The standardized anomaly of 1000–500-hPa thickness is calculated with respect to a 1979–2015 climatology [constructed using the methodology of Brammer and Thorncroft (2015, section 2a)]. The highest track density of CAO cold pools is found over northern areas of each region (Figs. 10a–f), indicating that CAO cold pools preferably impact these areas. However, the composite negative values of standardized anomaly of 1000–500-hPa thickness for each region show that anomalously cold air is found across the entire region (Figs. 10a–f), suggesting that anomalously cold air associated with the CAO cold pools may spread beyond the cold pool circle associated with the CAO cold pools and/or the CAO cold pools may be embedded in a broader area of anomalously cold air that is

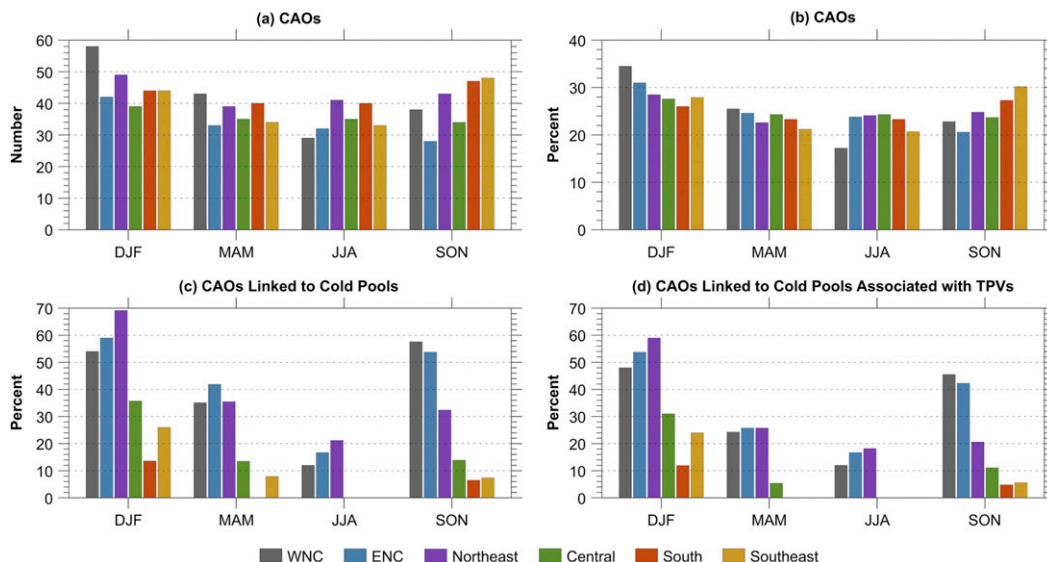


FIG. 12. (a) Normalized number of CAOs for each climate region and season found by normalizing the number of CAOs for each climate region and season (not shown) using the normalization procedure discussed in the beginning of section 3b. (b) Percentage of CAOs for each climate region occurring each season, where this percentage is defined as the number of CAOs for that climate region and season divided by the number of CAOs for that climate region. (c) Percentage of CAOs linked to cold pools for each climate region and season, where this percentage is defined as the number of CAOs linked to cold pools for that climate region and season divided by the number of CAOs for that climate region and season. (d) Percentage of CAOs linked to cold pools associated with TPVs for each climate region and season, where this percentage is defined as the number of CAOs linked to cold pools associated with TPVs for that climate region and season divided by the number of CAOs for that climate region and season. Seasons are defined in the Fig. 11 caption, where CAOs are separated into each season based on the month of their first date of occurrence.

also impacting the region. In addition, surface anticyclones that may accompany the CAO cold pools (e.g., Dallavalle and Bosart 1975; Colucci and Davenport 1987; Rogers and Rohli 1991) and terrain channeling (e.g., Bell and Bosart 1988; Colle and Mass 1995; Schultz et al. 1997) may help advect cold air equatorward across a region.

There is a southward shift of the preferred areas impacted by the CAO cold pools from northern regions of the United States (Figs. 10a–c) to southern regions of the United States (Figs. 10d–f), as indicated by a southward shift of the highest values of track density, and as suggested by a southward shift of the composite 540-dam contour of 1000–500-hPa thickness and of the composite negative values of standardized anomaly of 1000–500-hPa thickness. There is also an eastward shift of the preferred areas impacted by CAO cold pools from western regions of the United States (Figs. 10a,d), to central regions of the United States (Figs. 10b,e), and then to eastern regions of the United States (Figs. 10c,f), as indicated by an eastward shift of the highest values of track density, and as suggested by an eastward shift of a composite 1000–500-hPa thickness trough and of the composite negative values of standardized anomaly of 1000–500-hPa thickness. As an example of the documented eastward shift of the preferred areas impacted by CAO cold pools, it may be inferred that CAO cold pools impacting the Northeast (Fig. 10c) more often track east of the Great Lakes

compared to CAO cold pools impacting ENC, which more often track over or west of the Great Lakes (Fig. 10b). Cold pools located farther east and any accompanying surface anticyclone and associated northerly flow of cold air are less likely to pass over and be modified by the warmer Great Lakes (e.g., via surface sensible heat fluxes) than those located farther west, and thus are more likely to be colder upon reaching the Northeast.

d. Seasonality of TPVs, cold pools, and CAOs

Separating the climatologies of TPVs and cold pools by season, it is found that the highest and lowest number of all TPVs occurs during the winter and summer, respectively (Fig. 11a), and the highest and lowest number of all cold pools occurs during the summer and winter, respectively (Fig. 11b). Shortwave radiative heating, which may offset TPV intensification due to longwave radiative cooling (e.g., Cavallo and Hakim 2013) and which is smallest and largest during winter and summer in high latitudes, respectively, may contribute to the occurrence of the highest and lowest number of TPVs during winter and summer, respectively. Cold pools embedded in stronger horizontal thickness gradients during winter compared to summer may contribute to the occurrence of the lowest number of cold pools during winter and the highest number of cold pools during summer,

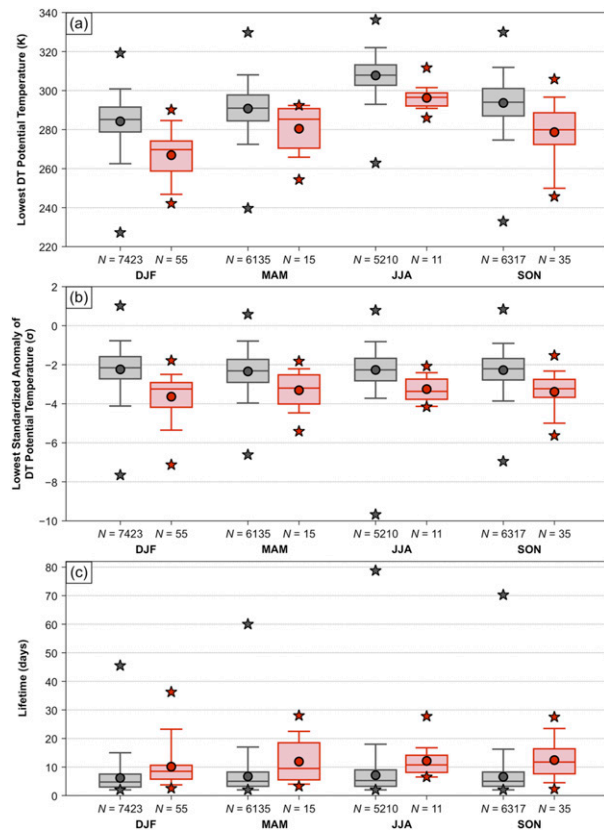


FIG. 13. Box-and-whisker plots showing a comparison between climatological TPVs (gray) and CAO TPVs (red) each season for the following characteristics: (a) lowest DT potential temperature (K) during the lifetime of the TPVs, (b) lowest standardized anomaly of DT potential temperature (σ) at the TPV center during the lifetime of the TPVs, and (c) lifetime of the TPVs (days). Boxes extend from the 25th to 75th percentiles, with median values denoted by solid line within each box. Whiskers extend to the 5th and 95th percentiles. Circles denote the mean values and stars denote the minimum and maximum values. Mean values are given in Table 6. The number of TPVs for each box-and-whisker plot is indicated. Seasons are defined in the Fig. 11 caption, where TPVs are separated into each season based on the month of their genesis date.

as such cold pools may appear as thickness troughs that are not trackable as cold pools.

The number of TPVs transported to middle latitudes is highest during the winter and lowest during the summer, when considering TPVs transported equatorward of crossing latitudes ranging from 60° to 45°N , every 5° (Fig. 11c). The number of cold pools transported to middle latitudes is highest during summer when considering crossing latitudes of 60° and 55°N , but lowest during summer when considering crossing latitudes of 50° and 45°N (Fig. 11d). The occurrence of the highest number of all cold pools during summer (Fig. 11b) likely contributes to the occurrence of the highest number of cold pools transported to middle latitudes during summer when considering crossing latitudes of 60° and 55°N (Fig. 11d). The more-poleward position of

the polar jet stream and increased shortwave radiative heating over middle and high latitudes during summer relative to other seasons likely contribute to the occurrence of the lowest number of TPVs transported to middle latitudes during summer when considering crossing latitudes of 60° – 45°N (Fig. 11c) and the lowest number of cold pools transported to middle latitudes during summer when considering crossing latitudes of 50° and 45°N (Fig. 11d). There is a substantial decrease in the number of TPVs and cold pools transported to middle latitudes as the crossing latitude decreases for a given season (Figs. 11c,d), suggesting that it may take an increasingly amplified flow pattern to enable TPVs and cold pools to be transported equatorward of a given crossing latitude as the crossing latitude decreases.

CAOs most often occur during the winter for all regions except South and Southeast (Figs. 12a,b). The greater occurrence of CAOs during winter compared to other seasons for all regions except South and Southeast likely is a consequence of the lower-latitude position of the polar jet stream and decreased shortwave radiative heating during winter relative to other seasons. Thus, cold air masses are more likely to develop and spread southward across the central and eastern United States and contribute to CAO development during winter. There is a higher percentage of CAOs linked to cold pools and CAOs linked to cold pools associated with TPVs over northern regions of the United States (i.e., WNC, ENC, and Northeast) compared to southern regions of the United States (i.e., Central, South, and Southeast) for all seasons (Figs. 12c,d), which likely is a consequence of the substantial decrease in the number of TPVs and cold pools crossing equatorward of a given crossing latitude as the crossing latitude decreases for a given season (Figs. 11c,d). There is a higher percentage of CAOs linked to cold pools and CAOs linked to cold pools associated with TPVs during winter compared to summer for all regions (Figs. 12c,d), which likely is a consequence of the transport of a higher number of TPVs and cold pools equatorward of 50° and 45°N during winter compared to summer (Fig. 11c,d).

e. Characteristics of TPVs and cold pools

Characteristics of CAO TPVs and CAO cold pools for all regions are now examined and compared to those of the full climatology of TPVs transported to middle latitudes and cold pools transported to middle latitudes (hereafter climatological TPVs and climatological cold pools), respectively, for each season. The characteristics of the TPVs that are examined are 1) lowest DT potential temperature during the lifetime of the TPVs, 2) lowest standardized anomaly of DT potential temperature at the TPV center during the lifetime of the TPVs, and 3) lifetime of the TPVs. The characteristics of the cold pools that are examined are 1) lowest 1000–500-hPa thickness during the lifetime of the cold pools, 2) lowest standardized anomaly of 1000–500-hPa thickness at the cold pool center during the lifetime of the cold pools, and 3) lifetime of the cold pools. Standardized anomalies are constructed as described in section 3c. The aforementioned

TABLE 6. A comparison between climatological (Climo) TPVs and CAO TPVs for each season of the number of TPVs and of the mean values of the following characteristics of the TPVs: 1) lowest DT potential temperature (θ ; K) during the lifetime of the TPVs, 2) lowest standardized anomaly of DT θ (σ) at the TPV center during the lifetime of the TPVs, and 3) lifetime of the TPVs (days). For each of the characteristics and each season, the mean value for the climatological TPVs is statistically significantly different from the mean value for the CAO TPVs at the 95% confidence level. Seasons are defined in the Fig. 11 caption, where TPVs are separated into each season based on the month of their genesis date.

	DJF		MAM		JJA		SON	
	Climo	CAO	Climo	CAO	Climo	CAO	Climo	CAO
Number	7423	55	6135	15	5210	11	6317	35
Lowest DT θ (K)	284.2	266.9	290.8	280.5	307.8	296.3	293.7	278.7
Lowest standardized anomaly of DT θ (σ)	-2.24	-3.64	-2.34	-3.31	-2.27	-3.25	-2.28	-3.38
Lifetime (days)	6.2	10.1	6.7	11.9	7.1	12.1	6.6	12.4

characteristics will illuminate whether there are differences in the coldness and longevity between CAO TPVs and climatological TPVs, and between CAO cold pools and climatological cold pools.

A bootstrap resampling with replacement test is adapted from Torn and Hakim (2015) and is used to determine if there are statistically significant differences between the mean value of each characteristic for each season between that of the CAO TPVs and that of the climatological TPVs. The bootstrap test is also used for CAO cold pools and climatological cold pools, but will be described only for TPVs. For each characteristic and each season, a sample of the climatological TPVs of size N , where N is equal to the number of CAO TPVs for that season, is randomly sampled and the mean value of that characteristic for that sample is determined. This process is repeated 10 000 times to yield a distribution of the mean value of that characteristic for the climatological TPVs. If the mean value of that characteristic for the CAO TPVs falls outside of the 95% confidence bounds of the distribution of the mean value of that characteristic for the climatological TPVs, the difference between the respective mean values is said to be statistically significant.

Compared to climatological TPVs, CAO TPVs are associated with a statistically significantly lower mean value of lowest DT potential temperature (Fig. 13a and Table 6) and of lowest standardized anomaly of DT potential temperature at the TPV center (Fig. 13b and Table 6) during the lifetime of the TPVs for all seasons. Compared to climatological cold pools, CAO cold pools are associated with a statistically significantly lower mean value of lowest 1000–500-hPa thickness (Fig. 14a and Table 7) and of lowest standardized anomaly of 1000–500-hPa thickness at the cold pool center (Fig. 14b and Table 7) during the lifetime of the cold pools for all seasons. Thus, CAO TPVs and CAO cold pools are statistically significantly colder than climatological TPVs and climatological cold pools, respectively, for all seasons.

The lowest standardized anomaly of DT potential temperature for some CAO TPVs and of 1000–500-hPa thickness for some CAO cold pools overlaps with the 25th–75th percentiles of the lowest standardized anomaly of DT potential temperature for climatological TPVs (Fig. 13b) and of 1000–500-hPa thickness for climatological cold pools (Fig. 14b), respectively, for all seasons. This overlap indicates that some CAO TPVs and some CAO cold pools are as anomalously cold as climatological TPVs and climatological cold pools, respectively,

suggesting that TPVs and cold pools that contribute to CAOs are not always exceptionally cold. The lowest DT potential temperature of climatological TPVs and CAO TPVs (Fig. 13a) and the lowest 1000–500-hPa thickness of climatological cold pools and CAO cold pools (Fig. 14a) exhibit greater seasonal variability than the lowest standardized anomaly of DT potential temperature of climatological TPVs and CAO TPVs (Fig. 13b) and the lowest standardized anomaly of 1000–500-hPa thickness of climatological cold pools and CAO cold pools (Fig. 14b). As an example of this difference in seasonal variability, it may be inferred that a CAO TPV during summer may not be as cold as a CAO TPV during winter, but the CAO TPVs may be similarly anomalously cold during both seasons.

In terms of longevity, CAO TPVs are characterized by a statistically significantly longer mean lifetime compared to climatological TPVs for all seasons (Fig. 13c and Table 6), and CAO cold pools are characterized by a statistically significantly longer mean lifetime compared to climatological cold pools for all seasons except spring (Fig. 14c and Table 7). The tendency for statistically significantly longer lifetimes of CAO TPVs and CAO cold pools compared to climatological TPVs and climatological cold pools, respectively, suggests that a longer period of longwave radiative cooling may be contributing to greater cooling of CAO TPVs and CAO cold pools compared to climatological TPVs and climatological cold pools, respectively. This greater cooling is consistent with the aforementioned result that CAO TPVs and CAO cold pools are statistically significantly colder than climatological TPVs (Figs. 13a,b and Table 6) and climatological cold pools (Figs. 14a,b and Table 7), respectively.

4. Summary

It is shown in prior studies that TPVs are associated with anomalously cold air throughout the depth of the troposphere (e.g., Cavallo and Hakim 2010) and that there is evidence of linkages between TPVs, cold pools, and CAOs (e.g., Boyle and Bosart 1983; Shapiro et al. 1987; Hakim et al. 1995; Papritz et al. 2019; Lillo et al. 2020). Additional evidence is provided in the present study of the linkages between TPVs, cold pools, and CAOs by comparing climatologies of TPVs, cold pools, and CAOs occurring in six NCEI-defined climate regions over the central and eastern United States, and identifying

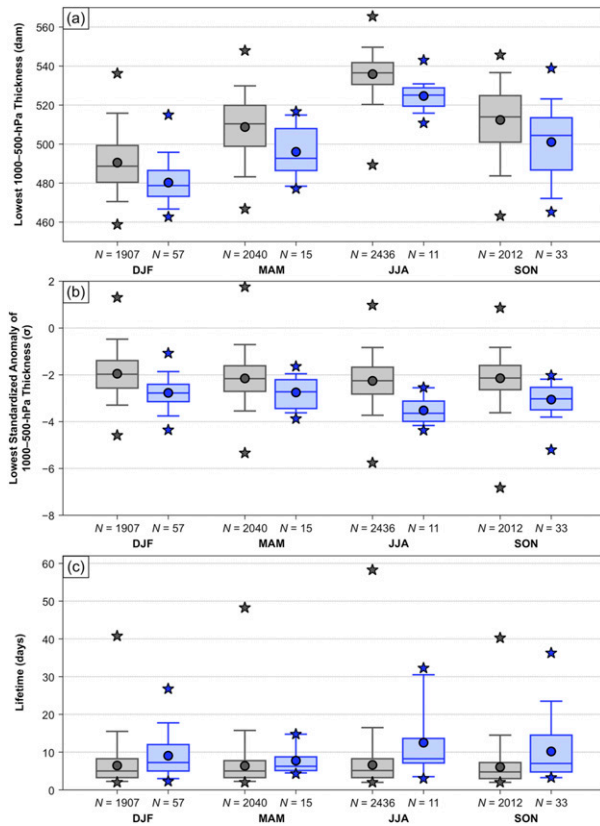


FIG. 14. Box-and-whisker plots showing a comparison between climatological cold pools (gray) and CAO cold pools (blue) each season for the following characteristics: (a) lowest 1000–500-hPa thickness (dam) during the lifetime of the cold pools, (b) lowest standardized anomaly of 1000–500-hPa thickness (σ) at the cold pool center during the lifetime of the cold pools, and (c) lifetime of the cold pools (days). Boxes extend from the 25th to 75th percentiles, with median values denoted by solid line within each box. Whiskers extend to the 5th and 95th percentiles. Circles denote the mean values and stars denote the minimum and maximum values. Mean values are given in Table 7. The number of cold pools for each box-and-whisker plot is indicated. Seasons are defined in the Fig. 11 caption, where cold pools are separated into each season based on the month of their genesis date.

CAOs linked to cold pools associated with TPVs for these regions.

It is shown in prior studies (e.g., Hakim and Canavan 2005; Cavallo and Hakim 2009, 2012) and in the present study that

central and eastern North America, in particular northern Canada and the Canadian Archipelago, are regions of high TPV occurrence, and it is also shown in the present study that they are regions of high cold pool occurrence. It is further shown in the present study that central and eastern North America is a preferred corridor for the equatorward transport of TPVs and cold pools to middle latitudes. Upper-tropospheric ridges and ridge amplification over the eastern North Pacific, western North America, the North Atlantic, Greenland, and the Arctic may allow TPVs and cold pools to move equatorward over central and eastern North America and to contribute to the development of CAOs over the central and eastern United States (e.g., Namias 1978; Shapiro et al. 1987; Alberta et al. 1991; Colle and Mass 1995; Hakim et al. 1995; Konrad 1996; Colucci et al. 1999; Waugh et al. 2017).

The percentage of CAOs linked to cold pools associated with TPVs is higher over northern regions of the United States (32.1%–35.7%) compared to southern regions of the United States (4.4%–12.5%), which is a consequence of the higher occurrence frequency of TPVs and cold pools over northern regions of the United States compared to southern regions of the United States, which likely is a consequence of the transport of a higher number of TPVs and cold pools equatorward of 50° and 45°N during winter compared to summer. TPVs and cold pools contributing to CAOs most frequently form over northern Canada and the Canadian Archipelago before generally traveling southeastward across Canada toward southern Canada and the northern United States.

TPVs and cold pools contributing to CAOs are statistically significantly colder for each season and statistically significantly longer lived for each season (except spring for cold pools) than climatological TPVs and cold pools, respectively. It is anticipated that longwave radiative cooling plays an important role in the intensification of TPVs and cold pools contributing to CAOs (e.g., Curry 1983; Emanuel 2008; Turner and Gyakum 2011; Cavallo and Hakim 2013; Papritz et al. 2019). Furthermore, a dynamical response to the intensification of a TPV may be the intensification of a cold pool beneath the TPV (e.g., Papritz et al. 2019), as is suggested by the concomitant intensification of the TPV and cold pool involved in the January 1982 CAO that is documented in the present study.

TABLE 7. A comparison between climatological (Climo) cold pools and CAO cold pools for each season of the number of cold pools and of the mean values of the following characteristics of the cold pools: 1) lowest 1000–500-hPa thickness (dam) during the lifetime of the cold pools, 2) lowest standardized anomaly of 1000–500-hPa thickness (σ) at the cold pool center during the lifetime of the cold pools, and 3) lifetime of the cold pools (days). For each of the characteristics and each season, the mean value for the climatological cold pools is statistically significantly different from the mean value for the CAO cold pools at the 95% confidence level, except where indicated by an asterisk. Seasons are defined in the Fig. 11 caption, where cold pools are separated into each season based on the month of their genesis date.

	DJF		MAM		JJA		SON	
	Climo	CAO	Climo	CAO	Climo	CAO	Climo	CAO
Number	1907	57	2040	15	2436	11	2012	33
Lowest thickness (dam)	490.5	480.3	508.8	496.0	535.9	524.7	512.4	501.0
Lowest standardized anomaly of thickness (σ)	-1.95	-2.77	-2.15	-2.75	-2.26	-3.52	-2.14	-3.06
Lifetime (days)	6.4	9.0	6.4*	7.8*	6.6	12.5	6.1	10.2

Acknowledgments. The authors thank Ron McTaggart-Cowan, Lukas Papritz, and one anonymous reviewer for constructive feedback on a prior version of this manuscript. The authors thank Nicholas Szapiro (Norwegian Meteorological Institute) and Steven Cavallo (University of Oklahoma) for providing TPVTrack code and for helpful discussions. The authors thank Zachary Murphy (WeatherWorks, LLC) for helpful discussions. This research was performed as part of the first author's M.S. thesis at the University at Albany, SUNY. This research was funded by NSF Grant AGS-1355960 and ONR Grant N00014-18-1-2200.

Data availability statement. The ERA-Interim data used in this study were downloaded from the ECMWF. Daily minimum temperature data used to identify CAOs were extracted from the GHCN-Daily dataset, which is available from NOAA NCEI. TPV and cold pool tracks, and data pertaining to the linkages between TPVs, cold pools, and CAOs, are available from the first author upon request.

REFERENCES

- Alberta, T. L., S. J. Colucci, and J. C. Davenport, 1991: Rapid 500-mb cyclogenesis and anticyclonogenesis. *Mon. Wea. Rev.*, **119**, 1186–1204, [https://doi.org/10.1175/1520-0493\(1991\)119<1186:RMCAA>2.0.CO;2](https://doi.org/10.1175/1520-0493(1991)119<1186:RMCAA>2.0.CO;2).
- Bell, G. D., and L. F. Bosart, 1988: Appalachian cold-air damming. *Mon. Wea. Rev.*, **116**, 137–161, [https://doi.org/10.1175/1520-0493\(1988\)116<0137:ACAD>2.0.CO;2](https://doi.org/10.1175/1520-0493(1988)116<0137:ACAD>2.0.CO;2).
- , and —, 1989: A 15-year climatology of Northern Hemisphere 500 mb closed cyclone and anticyclone centers. *Mon. Wea. Rev.*, **117**, 2142–2164, [https://doi.org/10.1175/1520-0493\(1989\)117<2142:AYCONH>2.0.CO;2](https://doi.org/10.1175/1520-0493(1989)117<2142:AYCONH>2.0.CO;2).
- Bosart, L. F., G. J. Hakim, K. R. Tyle, M. A. Bedrick, W. E. Bracken, M. J. Dickinson, and D. M. Schultz, 1996: Large-scale antecedent conditions associated with the 12–14 March 1993 cyclone (“Superstorm ’93”) over eastern North America. *Mon. Wea. Rev.*, **124**, 1865–1891, [https://doi.org/10.1175/1520-0493\(1996\)124<1865:LSACAW>2.0.CO;2](https://doi.org/10.1175/1520-0493(1996)124<1865:LSACAW>2.0.CO;2).
- Boyle, J. S., and L. F. Bosart, 1983: A cyclone/anticyclone couplet over North America: An example of anticyclone evolution. *Mon. Wea. Rev.*, **111**, 1025–1045, [https://doi.org/10.1175/1520-0493\(1983\)111<1025:ACCONA>2.0.CO;2](https://doi.org/10.1175/1520-0493(1983)111<1025:ACCONA>2.0.CO;2).
- Brammer, A., and C. D. Thorncroft, 2015: Variability and evolution of African easterly wave structures and their relationship with tropical cyclogenesis over the eastern Atlantic. *Mon. Wea. Rev.*, **143**, 4975–4995, <https://doi.org/10.1175/MWR-D-15-0106.1>.
- Cavallo, S. M., and G. J. Hakim, 2009: Potential vorticity diagnosis of a tropopause polar cyclone. *Mon. Wea. Rev.*, **137**, 1358–1371, <https://doi.org/10.1175/2008MWR2670.1>.
- , and —, 2010: Composite structure of tropopause polar cyclones. *Mon. Wea. Rev.*, **138**, 3840–3857, <https://doi.org/10.1175/2010MWR3371.1>.
- , and —, 2012: Radiative impact on tropopause polar vortices over the Arctic. *Mon. Wea. Rev.*, **140**, 1683–1702, <https://doi.org/10.1175/MWR-D-11-00182.1>.
- , and —, 2013: Physical mechanisms of tropopause polar vortex intensity change. *J. Atmos. Sci.*, **70**, 3359–3373, <https://doi.org/10.1175/JAS-D-13-088.1>.
- Cellini, M. P., J. E. Walsh, R. M. Rauber, and D. H. Portis, 2006: Extreme cold air outbreaks over the United States, the polar vortex, and the large-scale circulation. *J. Geophys. Res.*, **111**, D02114, <https://doi.org/10.1029/2005JD006273>.
- Colle, B. A., and C. F. Mass, 1995: The structure and evolution of cold surges east of the Rocky Mountains. *Mon. Wea. Rev.*, **123**, 2577–2610, [https://doi.org/10.1175/1520-0493\(1995\)123<2577:TSAEOC>2.0.CO;2](https://doi.org/10.1175/1520-0493(1995)123<2577:TSAEOC>2.0.CO;2).
- Colucci, S. J., and J. C. Davenport, 1987: Rapid surface anticyclonogenesis: Synoptic climatology and attendant large-scale circulation changes. *Mon. Wea. Rev.*, **115**, 822–836, [https://doi.org/10.1175/1520-0493\(1987\)115<0822:RSASCA>2.0.CO;2](https://doi.org/10.1175/1520-0493(1987)115<0822:RSASCA>2.0.CO;2).
- , D. P. Baumhefner, and C. E. Konrad, 1999: Numerical prediction of a cold-air outbreak: A case study with ensemble forecasts. *Mon. Wea. Rev.*, **127**, 1538–1550, [https://doi.org/10.1175/1520-0493\(1999\)127<1538:NPOACA>2.0.CO;2](https://doi.org/10.1175/1520-0493(1999)127<1538:NPOACA>2.0.CO;2).
- Curry, J., 1983: On the formation of continental polar air. *J. Atmos. Sci.*, **40**, 2278–2292, [https://doi.org/10.1175/1520-0469\(1983\)040<2278:OTFOCP>2.0.CO;2](https://doi.org/10.1175/1520-0469(1983)040<2278:OTFOCP>2.0.CO;2).
- Dallavalle, J. P., and L. F. Bosart, 1975: A synoptic investigation of anticyclonogenesis accompanying North American polar air outbreaks. *Mon. Wea. Rev.*, **103**, 941–957, [https://doi.org/10.1175/1520-0493\(1975\)103<0941:ASIOAA>2.0.CO;2](https://doi.org/10.1175/1520-0493(1975)103<0941:ASIOAA>2.0.CO;2).
- Danielsen, E. F., 1968: Stratospheric-tropospheric exchange based on radioactivity, ozone and potential vorticity. *J. Atmos. Sci.*, **25**, 502–518, [https://doi.org/10.1175/1520-0469\(1968\)025<0502:STEBOR>2.0.CO;2](https://doi.org/10.1175/1520-0469(1968)025<0502:STEBOR>2.0.CO;2).
- Dee, D. P., and Coauthors, 2011: The ERA-Interim reanalysis: Configuration and performance of the data assimilation system. *Quart. J. Roy. Meteor. Soc.*, **137**, 553–597, <https://doi.org/10.1002/qj.828>.
- Defant, F., and H. Taba, 1957: The threefold structure of the atmosphere and the characteristics of the tropopause. *Tellus*, **9**, 259–274, <https://doi.org/10.3402/tellusa.v9i3.9112>.
- Emanuel, K., 2008: Back to Norway: An essay. *Synoptic-Dynamic Meteorology and Weather Analysis and Forecasting: A Tribute to Fred Sanders, Meteor. Monogr.*, No. 55, 87–96, <https://doi.org/10.1175/0065-9401-33.55.87>.
- Gotaas, Y., and C. S. Benson, 1965: The effect of suspended ice crystals on radiative cooling. *J. Appl. Meteor.*, **4**, 446–453, [https://doi.org/10.1175/1520-0450\(1965\)004<0446:TEOSIC>2.0.CO;2](https://doi.org/10.1175/1520-0450(1965)004<0446:TEOSIC>2.0.CO;2).
- Hakim, G. J., 2000: Climatology of coherent structures on the extratropical tropopause. *Mon. Wea. Rev.*, **128**, 385–406, [https://doi.org/10.1175/1520-0493\(2000\)128<0385:COCSOT>2.0.CO;2](https://doi.org/10.1175/1520-0493(2000)128<0385:COCSOT>2.0.CO;2).
- , and A. K. Canavan, 2005: Observed cyclone–anticyclone tropopause vortex asymmetries. *J. Atmos. Sci.*, **62**, 231–240, <https://doi.org/10.1175/JAS-3353.1>.
- , L. F. Bosart, and D. Keyser, 1995: The Ohio Valley wave-merger cyclogenesis event of 25–26 January 1978. Part I: Multiscale case study. *Mon. Wea. Rev.*, **123**, 2663–2692, [https://doi.org/10.1175/1520-0493\(1995\)123<2663:TOVWMC>2.0.CO;2](https://doi.org/10.1175/1520-0493(1995)123<2663:TOVWMC>2.0.CO;2).
- Hartjenstein, G., and R. Bleck, 1991: Factors affecting cold-air outbreaks east of the Rocky Mountains. *Mon. Wea. Rev.*, **119**, 2280–2292, [https://doi.org/10.1175/1520-0493\(1991\)119<2280:FACAOE>2.0.CO;2](https://doi.org/10.1175/1520-0493(1991)119<2280:FACAOE>2.0.CO;2).
- Hoskins, B. J., M. E. McIntyre, and A. W. Robertson, 1985: On the use and significance of isentropic potential vorticity maps. *Quart. J. Roy. Meteor. Soc.*, **111**, 877–946, <https://doi.org/10.1002/qj.49711147002>.
- Keyser, D., and M. A. Shapiro, 1986: A review of the structure and dynamics of upper-level frontal zones. *Mon. Wea. Rev.*, **114**, 452–499, [https://doi.org/10.1175/1520-0493\(1986\)114<0452:AROTSA>2.0.CO;2](https://doi.org/10.1175/1520-0493(1986)114<0452:AROTSA>2.0.CO;2).
- Konrad, C. E., II, 1996: Relationships between the intensity of cold-air outbreaks and the evolution of synoptic and planetary-scale

- features over North America. *Mon. Wea. Rev.*, **124**, 1067–1083, [https://doi.org/10.1175/1520-0493\(1996\)124<1067:RBTIOC>2.0.CO;2](https://doi.org/10.1175/1520-0493(1996)124<1067:RBTIOC>2.0.CO;2).
- , and S. J. Colucci, 1989: An examination of extreme cold air outbreaks over eastern North America. *Mon. Wea. Rev.*, **117**, 2687–2700, [https://doi.org/10.1175/1520-0493\(1989\)117<2687:AEOECA>2.0.CO;2](https://doi.org/10.1175/1520-0493(1989)117<2687:AEOECA>2.0.CO;2).
- Lefevre, R. J., and J. W. Nielsen-Gammon, 1995: An objective climatology of mobile troughs in the Northern Hemisphere. *Tellus*, **47A**, 638–655, <https://doi.org/10.3402/tellusa.v47i5.11558>.
- Lillo, S. P., S. M. Cavallo, D. B. Parsons, and C. P. Riedel, 2020: The role of a tropopause polar vortex in the January 2019 Arctic outbreak. *33rd Conf. on Climate Variability and Change*, Boston, MA, Amer. Meteor. Soc., 5A.1, <https://ams.confex.com/ams/2020Annual/meetingapp.cgi/Paper/369323>.
- Menne, M. J., I. Durre, R. S. Vose, B. E. Gleason, and T. G. Houston, 2012: An overview of the global historical climatology network-daily database. *J. Atmos. Oceanic Technol.*, **29**, 897–910, <https://doi.org/10.1175/JTECH-D-11-00103.1>.
- Murphy, Z. B., 2017: A climatological and multiscale analysis of cold air outbreaks in the Northeast United States. M.S. thesis, Dept. of Atmospheric and Environmental Sciences, University at Albany, State University of New York, 91 pp.
- Namias, J., 1978: Multiple causes of the North American abnormal winter 1976–77. *Mon. Wea. Rev.*, **106**, 279–295, [https://doi.org/10.1175/1520-0493\(1978\)106<0279:MCOTNA>2.0.CO;2](https://doi.org/10.1175/1520-0493(1978)106<0279:MCOTNA>2.0.CO;2).
- Papritz, L., S. Pfahl, I. Rudeva, I. Simmonds, H. Sodemann, and H. Wernli, 2014: The role of extratropical cyclones and fronts for Southern Ocean freshwater fluxes. *J. Climate*, **27**, 6205–6224, <https://doi.org/10.1175/JCLI-D-13-00409.1>.
- , E. Rouges, F. Aemisegger, and H. Wernli, 2019: On the thermodynamic preconditioning of Arctic air masses and the role of tropopause polar vortices for cold air outbreaks from Fram Strait. *J. Geophys. Res. Atmos.*, **124**, 11 033–11 050, <https://doi.org/10.1029/2019JD030570>.
- Pyle, M. E., D. Keyser, and L. F. Bosart, 2004: A diagnostic study of jet streaks: Kinematic signatures and relationship to coherent tropopause disturbances. *Mon. Wea. Rev.*, **132**, 297–319, [https://doi.org/10.1175/1520-0493\(2004\)132<0297:ADSOJS>2.0.CO;2](https://doi.org/10.1175/1520-0493(2004)132<0297:ADSOJS>2.0.CO;2).
- Reed, R. J., and E. F. Danielsen, 1959: Fronts in the vicinity of the tropopause. *Arch. Meteor. Geophys. Bioklimatol.*, **A11**, 1–17, <https://doi.org/10.1007/BF02247637>.
- Rogers, J. C., and R. V. Rohli, 1991: Florida citrus freezes and polar anticyclones in the Great Plains. *J. Climate*, **4**, 1103–1113, [https://doi.org/10.1175/1520-0442\(1991\)004<1103:FCFAPA>2.0.CO;2](https://doi.org/10.1175/1520-0442(1991)004<1103:FCFAPA>2.0.CO;2).
- Sanders, F., 1988: Life history of mobile troughs in the upper westerlies. *Mon. Wea. Rev.*, **116**, 2629–2648, [https://doi.org/10.1175/1520-0493\(1988\)116<2629:LHOMTI>2.0.CO;2](https://doi.org/10.1175/1520-0493(1988)116<2629:LHOMTI>2.0.CO;2).
- Schultz, D. M., W. E. Bracken, L. F. Bosart, G. J. Hakim, M. A. Bedrick, M. J. Dickinson, and K. R. Tyle, 1997: The 1993 Superstorm cold surge: Frontal structure, gap flow, and tropical impact. *Mon. Wea. Rev.*, **125**, 5–39, [https://doi.org/10.1175/1520-0493\(1997\)125<0005:TSCSFS>2.0.CO;2](https://doi.org/10.1175/1520-0493(1997)125<0005:TSCSFS>2.0.CO;2).
- Shapiro, M. A., T. Hampel, and A. J. Krueger, 1987: The Arctic tropopause fold. *Mon. Wea. Rev.*, **115**, 444–454, [https://doi.org/10.1175/1520-0493\(1987\)115<0444:TATF>2.0.CO;2](https://doi.org/10.1175/1520-0493(1987)115<0444:TATF>2.0.CO;2).
- Simmonds, I., and I. Rudeva, 2012: The great Arctic cyclone of August 2012. *Geophys. Res. Lett.*, **39**, L23709, <https://doi.org/10.1029/2012GL054259>.
- Smith, E. T., and S. C. Sheridan, 2018: The characteristics of extreme cold events and cold air outbreaks in the eastern United States. *Int. J. Climatol.*, **38**, e807–e820, <https://doi.org/10.1002/joc.5408>.
- Szapiro, N., and S. Cavallo, 2018: TPVTrack v1.0: A watershed segmentation and overlap correspondence method for tracking tropopause polar vortices. *Geosci. Model Dev.*, **11**, 5173–5187, <https://doi.org/10.5194/gmd-11-5173-2018>.
- Torn, R. D., and G. J. Hakim, 2015: Comparison of wave packets associated with extratropical transition and winter cyclones. *Mon. Wea. Rev.*, **143**, 1782–1803, <https://doi.org/10.1175/MWR-D-14-00006.1>.
- Turner, J. K., and J. R. Gyakum, 2011: The development of Arctic air masses in Northwest Canada and their behavior in a warming climate. *J. Climate*, **24**, 4618–4633, <https://doi.org/10.1175/2011JCLI3855.1>.
- , —, and S. M. Milrad, 2013: A thermodynamic analysis of an intense North American Arctic air mass. *Mon. Wea. Rev.*, **141**, 166–181, <https://doi.org/10.1175/MWR-D-12-00176.1>.
- Uccellini, L. W., D. Keyser, K. F. Brill, and C. H. Wash, 1985: The Presidents' Day cyclone of 18–19 February 1979: Influence of upstream trough amplification and associated tropopause folding on rapid cyclogenesis. *Mon. Wea. Rev.*, **113**, 962–988, [https://doi.org/10.1175/1520-0493\(1985\)113<0962:TPDCOF>2.0.CO;2](https://doi.org/10.1175/1520-0493(1985)113<0962:TPDCOF>2.0.CO;2).
- Walsh, J. E., A. S. Phillips, D. H. Portis, and W. L. Chapman, 2001: Extreme cold outbreaks in the United States and Europe, 1948–99. *J. Climate*, **14**, 2642–2658, [https://doi.org/10.1175/1520-0442\(2001\)014<2642:ECOITU>2.0.CO;2](https://doi.org/10.1175/1520-0442(2001)014<2642:ECOITU>2.0.CO;2).
- Waugh, D. W., A. H. Sobel, and L. M. Polvani, 2017: What is the polar vortex and how does it influence weather? *Bull. Amer. Meteor. Soc.*, **98**, 37–44, <https://doi.org/10.1175/BAMS-D-15-00212.1>.
- Westby, R. M., and R. X. Black, 2015: Development of anomalous temperature regimes over the southeastern United States: Synoptic behavior and role of low-frequency modes. *Wea. Forecasting*, **30**, 553–570, <https://doi.org/10.1175/WAF-D-14-00093.1>.